RSC Advances

This article can be cited before page numbers have been issued, to do this please use: T. Keawin, N. Prachumrak, S. Namuangruk, S. Pansay, N. Kungwan, S. Maensiri, S. Jungsuttiwong, T. Sudyoadsuk and V. Promarak, *RSC Adv.*, 2015, DOI: 10.1039/C5RA07161E.

ROYAL SOCIETY OF CHEMISTRY

www.rsc.org/advances

View Article Online
DOI: 10.1039/C5RA07161E

RSC Advances

RSCPublishing

ARTICLE

Efficient bifunctional materials based on pyrene- and triphenylamine-functionalized dendrimers for electroluminescent devices

Cite this: DOI: 10.1039/x0xx00000x

Received 00th January 2012,
Accepted 00th January 2012

DOI: 10.1039/x0xx00000x

www.rsc.org/

T. Keawin,[a] N. Prachumrak,[b] S. Namuangruk,[c] S. Pansay,[a] N. Kungwan,[d] S. Maensiri,[e] S. Jungsuttiwong,[a] T. Sudyoadsuk[b] and V. Promarak[b*]

To realize highly efficient bifunctional blue-light emitting and hole-transporting materials for OLEDs, a series of pyrene- and triphenylamine-peripheral functionalized carbazole dendrimers, namely **G1PYR**, **G2PYR**, **G1TPA** and **G2TPA**, were designed, synthesized and characterized. Especially, **G2PYR** having four pyrene units substituted on the 2nd generation carbazole dendritic scaffold exhibited a strong blue emission with high T_g amorphous and good film-forming properties. Simple structured blue OLED (λ_{EL} = 463 nm) using **G2PYR** as emissive layer and Alq3-based green OLED (λ_{EL} = 512 nm) using **G2PYR** as hole-transporting layer with high luminance efficiencies (η) and low turn-voltages (V_{on}) of 5.89 cd A^{-1} and 3.1 V, and 5.15 cd A^{-1} and 2.6 V were attained, respectively.

Introduction

In the last decade, we have seen great efforts taken in the field of organic light-emitting diodes (OLEDs) to develop new materials as well as to optimize device fabrication conditions in order to realize commercial applications in full colour displays and solid-state lightings with high efficiency and long lifetime.[1] Among the established light-emitting (EL) materials, only red and green systems have shown satisfactory efficiencies, colour purity and lifetimes to be of commercial value. Because of the large band gap energy, the performance of blue electroluminescent emitters is usually inferior to those of green and red emitters. Despite many blue electroluminescent systems, including fluorenes and spirofluorenes,[2] metal complexes,[3] oxadiazoles,[4] distyrylarylene derivatives,[5] pyrenes,[6] anthracenes,[7] aromatic amines,[8] and heterocyclic compounds,[9] have been synthesized and investigated, developing blue-emitters exhibiting not only with high efficiency but also with simple fabrication method remains a key challenge. Particularly, pyrene-based blue fluorescent emitters have attracted large attention for OLEDs, because the photoluminescence quantum yield, carrier mobility, and the electron-injection ability of emitters made of pyrene are higher when compared to those of fluorene derivatives.[10] However, a weakness of pyrene is that its emission in the solid state is effectively suppressed due to the formation of excimers *via* π-π stacking.[11] Numerous efforts have been attempted to improve the photophysical properties of pyrene such as 3,6-dipyrenylcarbazole end capped oligofluorenes,[12] tetraarylpyrenes[13] and 9,9-bis-(3-(9-phenyl-carbazoyl))-2,7-dipyrenylfluorene,[14] pyrene-1,3-*alt*-calix[4]arene,[15] fluorene-substituted pyrenes,[16] 2,7-bispyrene-9,9-bis(4-diphenylaminophenyl)fluorenes,[17] pyrene-modified carbazole oligomers[18] and pyrene functionalized octavinylsilsesquioxane cores.[19] In terms of the device fabrication, solution-processed OLEDs fabricated using molecular amorphous materials will have great advantages, because the materials used are easy to synthesize and purify, while the fabrication method is convenient, low cost and allows large-scale manufacturing with less material usage.[20] Several chemical approaches have been investigated for the development of such thermally stable amorphous EL materials.[21] These lead to our design of new molecular materials combining the fine photoluminescent efficiency and electron-transporting ability of pyrene units[22] with the hole-transporting capability, high thermal stability and glass state-forming ability of carbazole dendritic scaffolds.[23] We deduced that the sterically congested carbazole dendritic platforms[24] in these molecules would avert the peripheral pyrene rings to undesirable self-quenching in the solid state as well as improve the physical properties of the molecule, thereby realizing pyrene systems with pure blue-light emitting and hole-transporting bifunctional aspects for simple structured solution-processed OLEDs.

Herein we report a detailed synthesis of a series of pyrene- and triphenylamine-functionalized carbazole dendrimers (Scheme 1) as well as their physical and photophysical properties. The investigation of the device fabrication and performance using these materials as an emissive layer and hole-transporting layer is also reported.

View Article Online
DOI: 10.1039/C5RA07161E

Results and discussion

Materials synthesis

Scheme 1 outlines the synthesis of the bifunctional pyrene- and triphenylamine-peripheral functionalized carbazole dendrimers, namely **G*n*PYR** (**G1PYR** and **G2PYR**) and **G*n*TPA** (**G1TPA** and **G2TPA**). Ullmann coupling of an available 3,6-dibromocarbazole **1** with carbazole (2.2 equiv.) in the presence of CuI/±*trans*-1,2-diaminocyclohexane as a catalyst K_3PO_4 as a base in toluene followed by bromination of the resultant **2** with NBS in THF afforded the tetrabromo 2nd generation carbazole dendritic platform **3** in a good yield. Suzuki cross coupling of the bromide scaffolds **1** and **3** with the excess amount of either pyrene-1-boronic acid or 4-(diphenylamino)phenylboronic acid catalyzed by $Pd(PPh_3)_4$/2M Na_2CO_3 (aq) in THF gave the target **G1PYR** (light green solid**)**, **G2PYR** (light green solid**)**, **G1TPA** (white solid**)** and **G2TPA** (white solid**)** in 85-91% yields. The structures and purities of the compounds were confirmed by ^{1}H NMR, ^{13}C NMR and MALDI-TOF MS. These newly synthesized dendrimers show good solubility in most organic solvents ensuring that their thin films could be fabricated by low-cost solution casting processes.

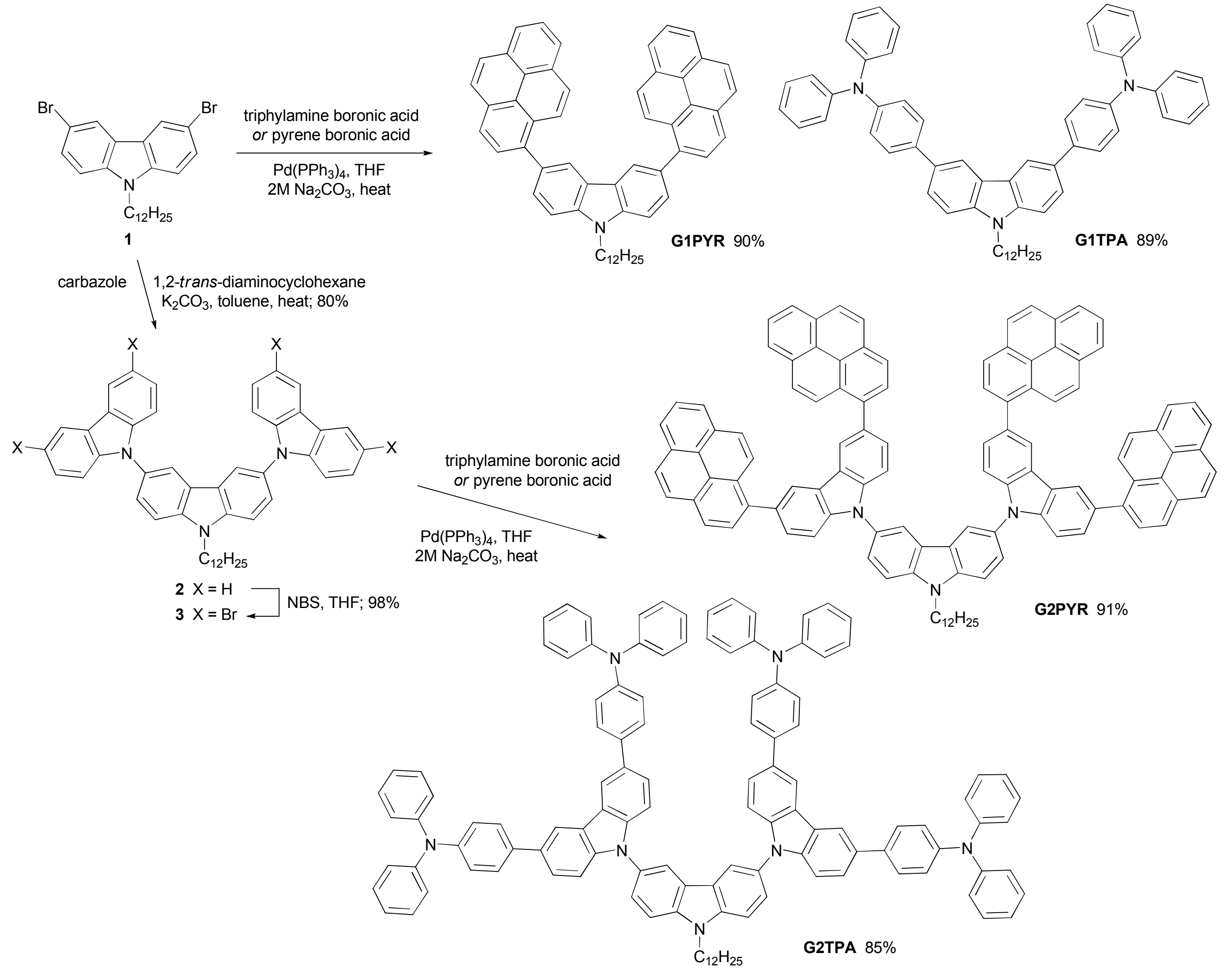

Scheme 1. Synthesis of **G*n*PYR** and **G*n*TPA**.

The quality and morphology of the spin-casting film, which is one of the key important factors for the OLEDs fabrication and performance, was exanimated by atomic force microscopy (AFM). Fig. 1 displays the tipping mode AFM images of the films spin-coated from $CHCl_3$:toluene solution of **G*n*PYR** and **G*n*TPA**. The AFM images of thin films of the 2nd generation dendrimers (**G2PYR** and **G2TPA**) show a very uniform and smooth surface, indicating excellent film-forming properties, while the surface of the spin-coated films of the 1st generation dendrimers (**G1PYR** and **G1TPA**) is a little coarser. These AFM images give evidence that the film uniformity is mostly determined by the generation or size of the dendrimers and in high-generation the dendrimer branches can relatively easily interpenetrate each other and establish intermolecular entanglements. Particularly, the spin-coated films of **G2PYR** and **G2TPA** are subjected to heating at 100 °C and inspected

View Article Online
DOI: 10.1039/C5RA07161E

by AFM periodically. The films remain unchanged after several hours. This is very important for the emissive materials to be thermally stable amorphous to avoid grain-boundary defects, which could reduce the efficiency of the OLEDs by hindering a charge migration.[25]

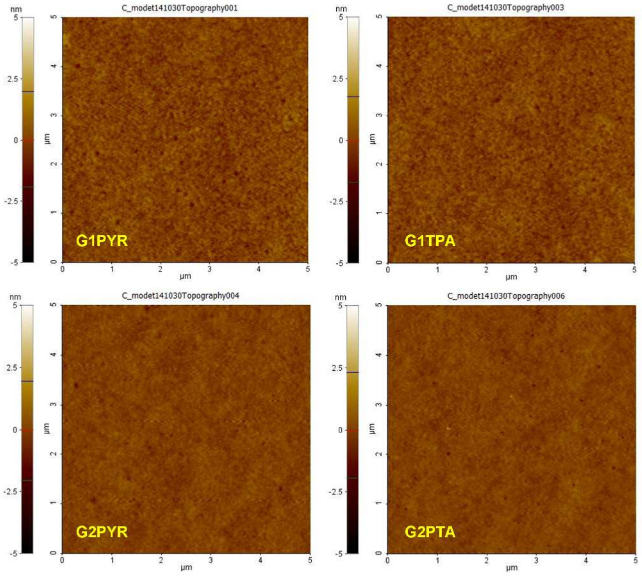

Fig. 1 Tapping mode AFM images of the spin-coated thin films.

Quantum chemical calculation

Quantum chemical calculations performed using the TD/B3LYP/6-31G (d,p) method[26] reveal that the 2nd generation dendritic dendrimers (**G2PYR** and **G2TPA**) adopt more sterically hindering molecular structures than their corresponding 1st generation dendrimers (**G1PYR** and **G1TPA**) (Fig. 2). Such structural characteristics could play an important role in reducing an undesirable intermolecular interaction in the solid state, and evolving the glass-forming ability and enhancing the thermal stability of the materials.[27] The distributions of π-electrons in the HOMOs of **G*n*PYR** and **G*n*TPA** are mainly on the 3,6-dipyrenylcarbazole and 3,6-bis[(diphenylamino)phenyl]carbazole moieties, respectively. In the LUMOs of **G*n*PYR**, the excited electrons are localized on the electron-rich pyrene peripheries, while in the LUMOs of **G*n*TPA** such electrons are located primarily on the central carbazole. Moreover, the DFT calculation also reveals that the S_1 state (S_0 → S_1 transition) of **G*n*TPA** is dominated by the HOMO → LUMO+1 transition, while the S_1 state of **G*n*PYR** is dominated by the HOMO → LUMO transition (see ESI (Table S2)). According to the DFT outcomes, it can be deduced that **G1PYR** and **G2PYR**, and **G1TPA** and **G2TPA** would have similar electronic properties with different physical properties.

Optical, thermal and electrochemical properties

The UV-vis absorption and photoluminescence PL spectra of **G*n*PYR** and **G*n*TPA** in CH_2Cl_2 solution and thin film are shown in Fig. 3 (Table 1). Both **G1PYR** and **G2PYR**, and **G1TPA** and **G2TPA** exhibit identical solution absorption spectra and optical band gaps (E_g^{opt}), indicating that increasing the size of the carbazole dendritic platforms has no or if any a little effect on the electronic properties of these molecules consistent with the DFT results. **G*n*PYR** and **G*n*TPA** feature a main absorption peak at 348 and 324 nm attributed to π-π* transitions of the 3,6-dipyrenylcarbazole and 3,6-bis[(diphenylamino)phenyl]carbazole groups, respectively. It is obvious that the absorption spectra of **G*n*PYR** exhibit a large red shift of 24 nm compared with those of **G*n*TPA**, which could be derived from the extended π conjugation in the 3,6-dipyrenylcarbazole. The PL spectra in solution and thin film of **G*n*PYR** and **G*n*TPA** show an emission peak in blue region. We found that the PL spectra of **G*n*PYR** in thin film are slightly red shifted (9-14 nm) to those in solution, indicating weak intermolecular interactions between **G*n*PYR** molecules in the solid state packing. This phenomenon may be caused by the planar structure of the 3,6-dipyrenylcarbazole moiety. With introducing the pyrene fluorophores (**G*n*PYR**, Φ_F = 0.94-0.95) to the surface of the dendrimers, the fluorescent quantum yield dramatically increased compared with the triphenylamine moieties (**G*n*TPA**, Φ_F = 0.57-0.61).

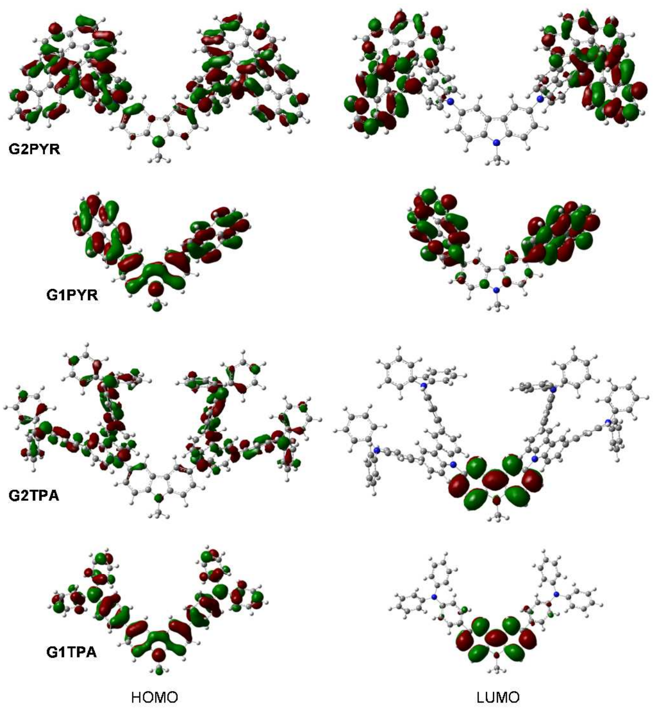

Fig. 2 HOMO and LUMO orbitals of **G*n*PYR** and **G*n*TPA** calculated by the B3LYP/6-31G(d,p) method in CH_2Cl_2.

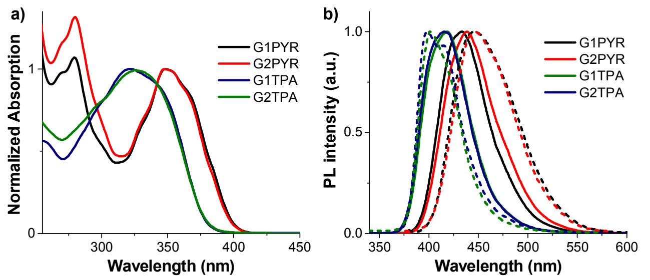

Fig. 3 a) UV-vis absorption and b) PL spectra measured in CH_2Cl_2 (solid line) and as spin-coated thin film (dotted line) on quarts substrates.

View Article Online
DOI: 10.1039/C5RA07161E

The thermal properties of **G*n*PYR** and **G*n*TPA** were determined by differential scanning calorimetry (DSC) and thermogravimetric analysis (TGA) (Fig. 4a and Table 1). TGAs reveal that their decomposition temperatures (T_{5d}) at 5 wt% weight loss are above 370 °C, showing the high thermal stability. DSCs (1st and 2nd heating scans) of the 2nd generation dendrimers, **G2PYR** and **G2TPA**, reveal a distinct glass transition temperature (T_g) at 211 and 145 °C, respectively, and no crystallization and melting peaks being observed at higher temperatures, indicating an excellent amorphous glass state stability.[31] DSC (1st heating scan) of **G1PYR** having smaller scaffold shows an endothermic baseline shift at 70 °C (T_g) followed by exothermic crystallization and endothermic melting peaks at 113 and 181 °C, respectively, while the DSC (1st heating scan) of **G1TPA** exhibits only a distinct melting peak at 186 °C. The subsequent DSC scan of **G1PYR** and **G1TPA** show only a T_g at 70 and 52 °C, respectively. The high T_gs of **G2PYR** and **G2TPA** may be attributed to the more bulky rigid structure of the 2nd generation carbazole dendritic skeleton. Operating temperatures of the OLEDs exceeding the T_g of the active organic materials are likely to promote thermally activated degradation processes and will induce device failure. Devices incorporating amorphous thin films having high T_g are less vulnerable to heat. Organic materials with high T_g are therefore highly desirable for applications in long lifetime electroluminescent devices.[28]

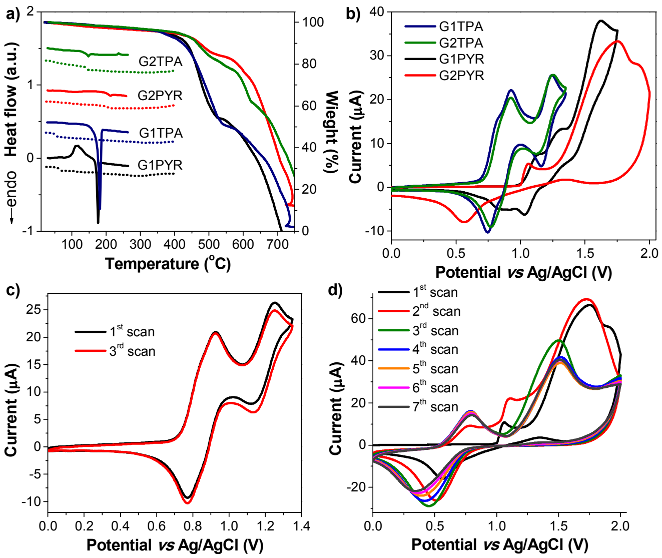

Fig. 4 a) DSC (1st heating (solid line) and 2nd heating (dotted line) scans) and TGA thermograms measured at a heating rate of 10 °C min^{-1} under N_2 flow. b) CV traces of **G*n*PYR** and **G*n*TPA** and repeated CV scans of c) **G2TPA** and d) **G2PYR** of measured in CH_2Cl_2/*n*-Bu_4NPF_6 at a scan rate of 50 mV s^{-1} under argon flow.

Table 1 Physical data of **G*n*PYR** and **G*n*TPA**.

Compd	λ_{abs} (log ε) (nm, M^{-1} cm^{-1})[a]	λ_{em}^{sol} (nm)[a]	λ_{em}^{film} (nm)[b]	Stokes shift (nm)[c]	Φ_F [d]	$T_g/T_c/T_m/T_{5d}$ (°C)[e]	$E_{1/2}$ *vs* Ag/AgCl (V)[f]	E_g^{opt}/E_g^{cal} (eV)[g]	HOMO/LUMO (eV)[h]
G1PYR	348 (3.80)	431	445	83	0.94	70/113/181/375	0.69 (E_{pc}), 0.93 (E_{pc}) 1.09, 1.26, 1.51	3.12/3.15	-5.45/-2.33
G2PYR	348 (3.88)	438	447	90	0.95	211/ - / - /400	0.57 (E_{pc}), 1.06 (E_{pa}), 1.66	3.12/3.15	-5.44/-2.32
G1TPA	324 (5.03)	415	398	94	0.57	52/ - /186/370	0.79, 0.89, 1.20	3.28/3.40	-5.15/-1.87
G2TPA	324 (5.14)	417	400	90	0.61	145/ - / - /417	0.81, 0.90, 1.19	3.28/3.31	-5.17/-1.89

[a] Measured in CH_2Cl_2. [b] Measured as a spin coated thin film. [c] Calculated from the difference between λ_{max} of emission spectra in solution and thin film. [d] Measured in CH_2Cl_2 with quinine sulphate in 0.1 M H_2SO_4 (Φ_F = 0.54) as a reference. [e] Obtained from DSC/TGA measured at 10 °C min^{-1} under N_2. [f] Obtained from CV measured in CH_2Cl_2/*n*-Bu_4NPF^6 (0.1 M) at scan rate of 50 m s^{-1}. [g] Calculated from $E_g^{opt} = 1240/\lambda_{onset}$; E_g^{cal} calculated by TD-B3LYP/6-31G(d,p) in CH_2Cl_2 solvent. [h] Calculated from HOMO = -(4.44 + E^{ox}_{onset}); LUMO = HOMO + E_g^{opt}.

The redox behaviours of **G*n*PYR** and **G*n*TPA** were investigated by means of cyclic voltammetry measurements (Fig. 4b-d and Table 1). CVs of **G*n*TPA** are nearly the same and display three quasi-reversible oxidation processes at $E_{1/2}$ of 0.8, 0.9 and 1.2 V. The first oxidation process assigns to the removal of electrons from the peripheral triphenylamine, resulting in radical cations. Vitally, the repeated CV scans of **G*n*TPA** reveal identical CV traces, suggesting they are electrochemically stable molecules. Under the same CV measurement conditions, on the contrary, **G*n*PYR** exhibit a series of irreversible oxidation processes and an additional peak at a lower potential on the cathodic scan (E_{pc}) around 0.57-0.69 V. Their repeated CV scans display an increasing change in the CV traces, signifying that a series of electrochemical reactions led to electro-polymerization of the radical cation species occurring on the glassy carbon electrode surface (Fig. S2).[6] However, this type of radical radical coupling reaction will become inactive in a non-diffusion system or in the device. In addition, under these measurement conditions, no reduction process is observed in all cases. The energy levels of the HOMO and LUMO of these compounds were determined and are listed in Table 1. Their HOMO levels, estimated from CV and optical results, are in the range of -5.15 to -5.45 eV, which are close to the work function of a commonly used indium tin oxide (ITO) anode (-4.80 eV). Their LUMO levels range from -1.87 eV to -2.33 eV, which are close to the work function of LiF/Al cathode (-2.60 eV).

Electroluminescence (EL) properties

AS BLUE LIGHT-EMITTING MATERIALS

Owing to their strong blue fluorescence (Φ_F > 0.94) and high HOMO levels (5.4 eV), **G*n*PYR** as hole-transporting non-doped blue emitters was first investigated and compared with a commercially available blue emitter, *N,N′*-diphenyl-*N,N′*-bis(1-

View Article Online
DOI: 10.1039/C5RA07161E

naphthyl)-(1,1'-biphenyl)-4,4'-diamine (NPB). The double-layer solution processed OLEDs (devices I-III) with the device structure of ITO/PEDOT:PSS/**G*n*PYR**(40 nm)/BCP(40 nm)/LiF(0.5 nm):Al(150 nm) were fabricated (Fig. 5a). **G*n*PYR** as the light-emitting layer (EML) were spin-coated from $CHCl_3$:toluene (1:1) solution. Conductive poly(3,4-ethylenedioxythiophene):poly(4-styrenesulfonate) (PEDOT: PSS) as hole injection layer and 2,9-dimethyl-4,7-diphenyl-1,10-phenanthroline (BCP) as hole blocking layer were incorporated to enable high efficiency diodes.[29] The electroluminescence data of the devices are shown in Fig. 6 and 7 and listed in Table 2. Under a bias voltage, all devices (I-III) emit a strong blue emission with λ_{EL} peaked at 437, 463 and 430 nm and a narrow FWHM of 67-90 nm, respectively (Fig. 7a). The electroluminescence (EL) spectra of devices I-II match with their corresponding PL spectra, indicating that the EL purely originates from **G*n*PYR** layers. Both devices I-II show a pure blue emission with CIE color coordinates of (0.15, 0.13) and (0.15, 0.16), respectively. Upon varying the bias voltages, no emission shoulder at the longer wavelength and no significant change in the EL spectra of devices I-II causing by the emission of the excimer and exciplex species formed at the EML/BCP interface, which often occurs in the devices fabricated from EML with planar molecular structure, is noticed.[30] In our case, the formation of such species could be prohibited by the bulky nature of the carbazole dendrimer implemented as molecular platform. As depicted in Fig 7, **G*n*PYR**-based blue OLEDs (devices I-II) show superior luminance efficiency than that of the reference NPB-based blue device (device III). The light turn-on voltage (V_{on}) at 1 cd m^{-2} of these devices is 3.1 V and the operating voltage (V_{100}) at 100 cd m^{-2} is in the range of 4.4-5.1 V, signifying a decent device performance. **G2PYR**-based diode (device II) exhibits the best device performance with a maximum brightness (L_{max}) of 23003 cd m^{-2}, a maximum luminance efficiency (η_{max}) of 5.89 cd A^{-1}, a maximum power efficiency (PE) of 2.67 lm W^{-1} and a high external quantum efficiency (EQE) of 6.81%. **G1PYR**-based diode (device I) shows a slightly lower device performance with an L_{max} of 11964 cd m^{-2}, a η_{max} of 3.67 cd A^{-1}, a PE of 1.68 lm W^{-1} and an EQE of 5.11%. The higher EL efficiency of the **G2PYR**-based device than **G1PYR**-based device may stem from a combination of a better thin film-forming quality and stability of **G2PYR**.[31]

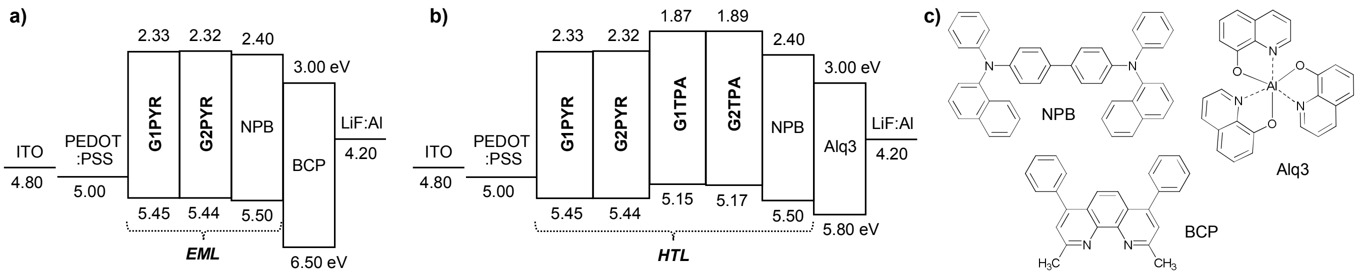

Fig. 5 Schematic energy diagrams of the OLEDs fabricated with a) **G*n*PYR** as EML and b) with **G*n*PYR** and **G*n*TPA** as HTL. c) Molecular structures of NPB, Alq3 and BCP.

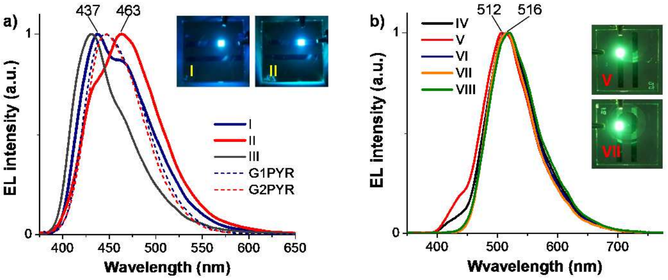

Fig. 6 Thin film PL spectra (dotted line) of the EML and EL spectra (solid line) of the OLEDs fabricated with a) **G*n*PYR** as EML and b) with **G*n*PYR** and **G*n*TPA** as HTL, and their emission colours under applied voltages.

AS HOLE-TRANSPORTING MATERIALS

According to the above mentioned properties of **G*n*PYR** and **G*n*TPA** including easily oxidized, absorbing in blue region and having a fairly shallow HOMO energy level (-5.15−-5.45 eV), they can serve as hole-transporting materials (HTM) to provide a hole-conductive (*via* charge hopping) pathway for positive charge carriers to migrate from the anode into the EML. To test this postulate, double-layer Alq3-based green OLEDs (devices IV-VII) with the structure of ITO/PEDOT:PSS/**G*n*PYR** and **G*n*TPA**(spin-coating)/Alq3(50 nm)/LiF(0.5 nm):Al(150 nm) were fabricated and investigated, where **G*n*PYR** and **G*n*TPA** were used as hole-transporting layers (HTL) and tris(8-hydroxyquinoline)aluminium (Alq3) as the green light-emitting (EML) and electron-transporting layers (ETL) (Fig. 5b-c). The reference diode (device VIII) fabricated with a commercial HTM, NPB, as HTL was prepared for comparison. The detailed EL data of the devices are shown in Fig. 6 and 7, and summarized in Table 2. All devices IV-VII under an applied voltage emit a bright green luminescence (λ_{EL} = 512-517 nm) (Fig. 6b). The EL spectra match well with the PL spectrum of Alq3, and the EL of the reference device III and other reported devices.[32] No emission at longer wavelengths owing to exciplex species formed at the HTL/Alq3 interface is also detected. From these results, and in view of the fact that a barrier for electron-migration at the Alq3/HTL interface is larger than that for hole-migration at the HTL/Alq3 interface (Fig. 5b), **G*n*PYR** and **G*n*TPA** will serve only as HTL, and Alq3 will act preferably as an electron blocker more than as a hole blocker and charge recombination thus con-fines to Alq3 layer. More importantly, a stable emission is obtained from these diodes in which the EL spectra and CIE coordinates did not change over the whole applied voltages. Devices VII and V using the 2nd generation dendrimers, **G2PYR** and **G2TPA**, as HTL exhibit excellent device performance with L_{max} of 27787-33846 cd m^{-2} for green OLED at 9.8-10.6 V, low V_{on} of 2.6-2.7 V, η_{max} of 5.15-6.10 cd A^{-1}, PE of 3.84-4.64 lm W^{-1} and EQE of 1.28-1.51%. The operating voltage at 100 cd m^{-2} of these diodes is as low as 3.4 V. The green OLEDs (devices IV, VI) fabricated with **G1PYR** and **G1TPA** as HTL show a slightly lower device performance with η_{max} of 4.48-4.79 cd A^{-1}, PE of 3.37-3.86 lm W^{-1} and EQE of 1.11-1.19%. Better film forming ability and quality of **G2PYR** and **G2TPA** may be the key to their superior hole-transport property and performance to those of devices using **G1PYR** and **G1TPA**. By comparison the performance of both devices VII and V with the reference NPB-based device VIII, the integration of either **G2PYR** or **G2TPA** in the device as HTL not only increases the η_{max} from to 4.89 cd A^{-1} to 5.15-6.10 cd A^{-1}, but also decreases the V_{on} from 2.8 to 2.6 V, indicating an excellent solution-processed HTM ability of both materials. Besides, the ability as amorphous HTM of **G2PYR** and **G2TPA** in terms of thermal stability of amorphous films (T_g = 145-211 °C) is also superior than commonly used NPB (T_g = 100 °C).

Although the luminance efficiency of **G2PYR**-based OLEDs as both EML and HTL cannot compete with reported iridium complex-based phosphorescent OLEDs (η_{max} = 53.5 cd A^{-1} and EQE = 20.1%)[33] and some thermally activated delayed fluorescence (TADF) OLEDs (EQE = 14.5%),[34] surely the advantage of the blue and green OLEDs in this study is a simple device fabrication process and structure. Wang *et al.* have reported pyrene derivatives as blue-light emitting and hole-transporting bifunctional materials. They exhibit a luminance efficiency of 0.97 cd A^{-1} with wavelength at 440 nm when used as a blue emitter and a luminance efficiency of 0.40 cd A^{-1} with wavelength at 453 nm when used as a hole-transporting material.[35] verifying that the ability of **G2PYR** as a non-doped hole-transporting blue emitter, in terms of device performance, is excellence. The performance of **G2PYR** is also better than our recent reported anthracene- and oligofluorene-cored carbazole dendrimer-based bifunctional materials.[36]

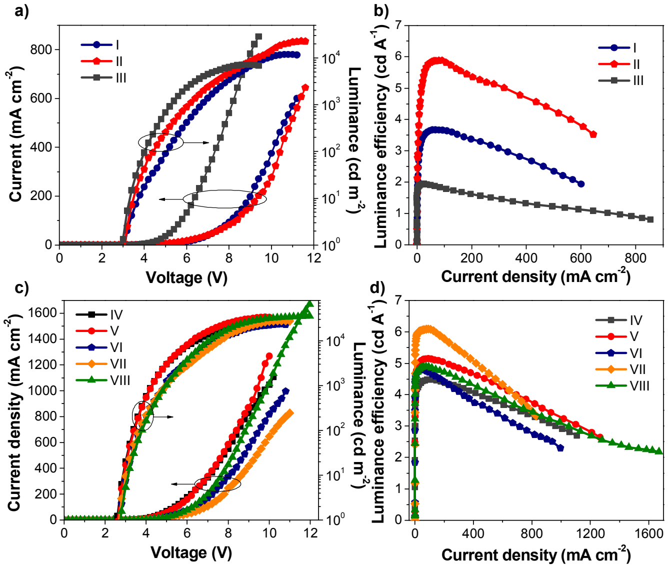

Fig. 7 Plots of a) and c) current density-luminance-voltage (*J-V-L*), and b) and d) efficiency-current density (η-*J*) characteristics of the OLEDs.

Table 2 Electroluminescent data of the OLEDs.

Device	EML/HTL	λ^{EL}_{max}/FWHM (nm)	V_{on}/V_{100} (V)[c]	L_{max} at voltage (cd m^{-2}/V)[d]	J_{max} (mA cm^{-2})[e]	η_{max}/η at L_{100}/η at L_{1000} (cd A^{-1})[f]	EQE (%)[g]	PE at voltage (lm W^{-1}/V)[h]	CIE (x,y)
I[a]	G1PYR	437, 463sh/83	3.1/5.1	11964 (10.8)	533	3.67/2.47/3.55	5.11	1.68 (6.2)	0.15, 0.13
II[a]	G2PYR	433sh, 463/90	3.1/4.4	23003 (11.4)	607	5.89/3.00/5.22	6.81	2.67 (6.8)	0.15, 0.16
III[a]	NPB	430/67	3.0/4.1	7189 (9.0)	822	1.95/1.85/1.90	2.72	1.61 (3.2)	0.16, 0.09
IV[b]	G1PYR	517/82	2.6/3.4	31201 (10.0)	1057	4.48/3.65/4.30	1.11	3.37 (3.4)	0.27, 0.50
V[b]	G2PYR	512/82	2.6/3.4	33846 (9.8)	1209	5.15/4.20/4.94	1.28	3.84 (3.5)	0.25, 0.46
VI[b]	G1TPA	515/83	2.7/3.7	23580 (10.6)	939	4.79/4.40/4.70	1.19	3.86 (3.4)	0.27, 0.53
VII[b]	G2TPA	516/82	2.7/3.7	27787 (10.6)	764	6.10/5.40/5.92	1.51	4.64 (3.4)	027, 0.54
VIII[b]	NPB	519/83	2.8/3.8	35631 (12.0)	1670	4.89/4.33/4.75	1.21	3.72 (3.6)	0.29, 0.53

[a] ITO/PEDOT:PSS/**EML**/BCP/LiF:Al. [b] ITO/PEDOT:PSS/**HTL**/Alq3/LiF:Al. [c] Turn-on voltages at 1 and 100 cd m^{-2}. [d] Maximum luminance at applied voltage. [e] Current density. [f] Luminance efficiencies at maximum, at luminance of 100 and 1000 cd m^{-2}. [g] Maximum external quantum efficiency. [h] Maximum power efficiency at applied voltage.

Experimental

Materials and methods

All starting materials were obtained from commercial suppliers and used without further purification; solvents were purified according to standard techniques. Compound **1** was synthesized following the reported procedure.[37]

^{1}H and ^{13}C NMR spectra were recorded on an AVANCE 300 MHz spectrometer. UV-Vis spectra were recorded on an UV Lambda 25 spectrometer. Photoluminescence spectra and fluorescence quantum yields (Φ_F) were measured with a LS 50B Luminescence spectrometer. Differential scanning calorimetry (DSC) and thermal gravimetric analysis (TGA) were performed on a DSC823e and TG-DTA 8120 thermal analyzers, respectively, with heating rate of 10 °C min^{-1} under N_2 flow. Cyclic voltammetry (CV) was carried out on a PGSTAT 12 with a three electrode system (platinum counter electrode, glassy carbon working electrode and Ag/AgCl reference electrode) at scan rate of 50 mV s^{-1} in the presence of

View Article Online
DOI: 10.1039/C5RA07161E

n-Bu_4NPF_6 as a supporting electrolyte in CH_2Cl_2 under argon flow. Melting points were measured using an Electrothermal IA 9100 series of digital melting point instrument and are uncorrected. High-resolution mass spectrometry (HRMS) analysis was performed on an Autoflex II MALDI-TOF/TOF mass spectrometer. The atomic force microscopy (AFM) analysis was performed on an XE 100.

All calculations were performed by Gaussian 09 code in CH_2Cl_2 solvent.[26] The energy or geometry optimizations were done by B3LYP/6-31G(d,p) method. The ground to excited state excitation energies were calculated by TD-B3LYP/6-31G(d,p) in CH_2Cl_2.

Materials synthesis

3,6-BIS(CARBAZOL-*N′*-YL)-*N*-DODECYLCARBAZOLE (2): A mixture of **1** (2.00 g, 4.04 mmol), carbazole (1.49 g, 8.89 mmol), CuI (0.38 g, 2.02 mmol), K_3PO_4 (2.14 g, 10.10 mmol) and ±*trans*-1,2-diaminocyclohexane (0.23 g, 2.10 mmol) in toluene (50 ml) was stirred at refluxed under N_2 for 24 h. After cooling, water (30 ml) was added and the mixture was extracted with CH_2Cl_2 (50 ml x 2). The combined organic phase was washed water (50 ml x 2), brine solution (50 ml), dried over anhydrous Na_2SO_4, filtered and removed to dryness. Purification by column chromatography over silica gel eluting with a mixture of CH_2Cl_2 and hexane (1:4) followed by recrystallization with a mixture of CH_2Cl_2 and CH_3OH afforded the product (2.15 g, 80%) as colorless solids: m.p. 232 °C; ^1H NMR (300 MHz, $CDCl_3$) δ 8.26 (2H, s), 8.21 (4H, d, J = 7.80 Hz), 7.68 (4H, s), 7.47-7.41 (8H, m), 7.36-7.28 (4H, m), 4.49 (2H, t, J = 7.20 Hz), 2.06 (2H, t, J = 6.90 Hz), 1.56-1.33 (18H, m), 0.93 (3H, t, J = 6.30 Hz) ppm; ^{13}C NMR (300 MHz, $CDCl_3$) δ 141.91, 129.35, 125.98, 125.87, 123.15, 120.29, 119.86, 110.13, 109.77, 43.15, 31.94, 29.67, 29.61, 29.51, 29.38, 29.21, 27.46, 22.86, 14.29 ppm; MALDI-TOF (*m/z*) (M^+) calcd for $C_{48}H_{47}N_3$: 665.9069, found 665.4128.

3,6-BIS(3′,6′-DIBROMOCARBAZOL-*N′*-YL)-*N*-DODECYLCARBAZOLE (3): To a stirred solution of **2** (1.00 g, 1.50 mmol) in THF (60 ml) in the dark was added NBS (1.10 g, 6.16 mmol) in small portions. The mixture was allowed to stir for 5 h. Water (15 ml) was added and the mixture was extracted with CH_2Cl_2 (50 ml x 2). The combined organic phase was washed with bine solution (50 ml), dried over anhydrous Na_2SO_4, filtered and removed to dryness. Purification by column chromatography over silica gel eluting with a mixture of CH_2Cl_2 and hexane (1:4) followed by recrystallization with a mixture of CH_2Cl_2 and CH_3OH gave the product (1.43 g, 98%) as white solids: m.p. 150 °C; ^1H NMR (300 MHz, $CDCl_3$) δ 8.21 (4H, s), 8.16 (2H, s), 7.68 (2H, d, J = 8.70 Hz), 7.57 (2H, d, J = 8.70 Hz), 7.48 (4H, d, J = 8.55 Hz), 7.22 (4H, d, J = 8.70 Hz), 4.49 (2H, t, J = 7.20 Hz), 2.04 (2H, t, J = 6.90 Hz), 1.57-1.27 (18H, m), 0.87 (3H, t, J = 6.30 Hz) ppm; ^{13}C NMR (300 MHz, $CDCl_3$) δ 140.82, 140.45, 129.33, 128.46, 126.61, 125.78, 123.32, 123.21, 119.72, 112.85, 111.48, 110.45, 43.78, 31.92, 29.64, 29.58, 29.46, 29.35, 29.17, 27.41, 22.69, 14.12 ppm; MALDI-TOF (*m/z*) (M^+) calcd for $C_{48}H_{43}Br_4N_3$: 977.0190, found 977.1070.

SYNTHESIS OF G*n*PYR AND G*n*TPA

A mixture of **1** or **3** (0.61 mmol), pyrene-1-boronic acid or 4-(diphenylamino)phenylboronic acid (1.40-3.10 mmol), $Pd(PPh_3)_4$ (0.02 mmol) and 2M Na_2CO_3 solution (7 ml) in THF (25 ml) was degased with N_2 for 5 min. The mixture was refluxed under N_2 for 48 h. After cooling, water (30 ml) was added and the mixture was extracted with CH_2Cl_2 (50 ml x 2). The combined organic layer was washed with water (50 ml), brine solution (50 ml), dried over anhydrous Na_2SO_4, filtered and removed to dryness. Purification by column chromatography over silica gel eluting with a mixture of CH_2Cl_2 and hexane (1:4) followed by recrystallization with a mixture of CH_2Cl_2 and CH_3OH yielded:

G1PYR as light green solids (90%): m.p. 200 °C; ^1H NMR (300 MHz, $CDCl_3$) δ 8.41 (2H, s), 8.34 (2H, d, J = 9.30 Hz), 8.25 (2H, d, J = 7.80 Hz), 8.20-8.10 (10H, m), 8.06-7.97 (4H, m), 7.79 (2H, d, J = 8.40 Hz), 7.66 (2H, d, J = 7.64 Hz), 4.47 (2H, t, J = 7.20 Hz), 2.06 (2H, q, J = 6.90 Hz), 1.57-1.30 (18H, m), 0.91 (3H, t, J = 6.90 Hz) ppm; ^{13}C NMR (300 MHz, $CDCl_3$) δ 140.31, 138.68, 132.10, 131.58, 131.10, 130.29, 128.89, 128.76, 128.25, 127.51, 127.32, 127.17, 125.93, 125.74, 125.11, 125.04, 124.93, 124.66, 123.11, 122.48, 108.71, 43.55, 31.96, 30.93, 29.69, 29.55, 29.40, 29.25, 27.50, 22.73, 14.16 ppm; MALDI-TOF (*m/z*) (M^+) calcd for $C_{56}H_{49}N$: 735.3865, found 735.2479.

G2PYR as light green solids (91%): m.p. >250 °C; ^1H NMR (300 MHz, $CDCl_3$) δ 8.49 (6H, s), 8.33 (4H, d, J = 9.3 Hz), 8.22 (4H, d, J = 7.8 Hz), 8.19-8.05 (20 H, m), 8.02 (4H, d, J = 3.0 Hz), 7.98 (4H, d, J = 7.8 Hz), 7.88 (2H, d, J = 8.4 Hz), 7.80-7.74 (6H, m), 7.68 (4H, d, J = 8.4 Hz), 4.55 (2H, bs), 2.11 (2H, bs), 1.48 (2H, bs), 1.27 (16H, bs), 0.86 (3H, t, J = 6.6 Hz) ppm; ^{13}C NMR (300 MHz, $CDCl_3$) δ 141.80, 140.45, 138.57, 133.09, 131.55, 131.06, 130.34, 129.40, 129.07, 128.89, 128.20, 127.48, 127.37, 127.19, 126.05, 125.92, 125.68, 125.07, 125.00, 124.94, 124.68, 124.64, 123.62, 123.46, 122.42, 119.97, 110.39, 109.84, 43.83, 31.92, 30.92, 29.66, 29.63, 29.53, 29.36, 29.26, 27.49, 22.69, 14.11 ppm; MALDI-TOF (*m/z*) (M^+) calcd for $C_{112}H_{79}N_3$: 1465.6274, found 1465.5541.

G1TPA as white solids (89%): m.p. 200 °C; ^1H NMR (300 MHz, $CDCl_3$) δ 8.36 (2H,s), 7.73 (2H, dd, J = 8.40 Hz, J = 1.2 Hz), 7.64 (2H, d, J = 8.40 Hz), 7.47 (2H, d, J = 8.40 Hz), 7.33-7.28 (8H, m), 7.24-7.18 (12H, m), 7.07 (4H, t, J = 7.20 Hz), 4.34 (2H, t, J = 7.20 Hz), 1.93 (2H, q, J = 6.90 Hz), 1.52-1.29 (18H, m), 0.90 (3H, t, J = 6.90 Hz) ppm; ^{13}C NMR (300 MHz, $CDCl_3$) δ 147.92, 146.43, 140.24, 136.51, 131.94, 129.27, 127.92, 125.10, 124.99, 124.54, 124.22, 123.56, 122.71, 118.48, 109.06, 43.37, 31.95, 29.74, 29.55, 29.46, 29.36, 29.10, 27.37, 22.72, 14.15 ppm; MALDI-TOF (*m/z*) (M^+) calcd for $C_{60}H_{59}N_3$: 821.4709, found 821.1257.

G2TPA as white solids (85%). m.p. >250 °C; ^1H NMR (300 MHz, $CDCl_3$) δ 8.39 (4H, s), 8.30 (2H, s), 7.72 (6H, s), 7.65-7.60 (12H, m), 7.45 (6H, d, J = 8.40 Hz), 7.30-7.25 (16H, m), 7.20-7.15 (20H, m), 7.03 (8H, t, J = 7.20 Hz), 4.52 (2H,t, J = 7.20 Hz), 2.16-2.06 (2H, m), 1.61-1.26 (18H, m), 0.89 (3H, t, J = 6.90 Hz) ppm; ^{13}C NMR (300 MHz, $CDCl_3$) δ 147.85, 146.49, 141.58, 140.25, 136.37, 132.88, 130.87, 129.36, 123.223, 128.81, 127.93, 125.84, 125.26, 124.45, 124.20, 123.83, 123.45, 122.69, 119.70, 118.39, 110.10, 43.79, 38.76, 31.92, 30.90, 30.39, 29.70, 29.65, 29.36, 28.94, 27.45, 23.77, 22.98, 22.69, 14.11 ppm; MALDI-TOF (*m/z*) (M^+) calcd for $C_{120}H_{99}N_7$: 1637.7962, found 1637.4813.

OLED fabrication and testing

All OLED devices using **G*n*PYR** and **G*n*TPA** as hole-transporting layer (THL) and **G*n*PYR** as blue emissive layer (EML) with the device structures of ITO/PEDOT:PSS/THL(spin-coating)(30-40 nm)/Alq3(50 nm)/LiF(0.5 nm):Al(150 nm) and ITO/PEDOT:PSS/EML(spin-coating)(30-40 nm)/BCP(40 nm)/LiF(0.5 nm):Al(150 nm) were fabricated and characterized as followed. Thin films of **G*n*PYR** and **G*n*TPA** were deposited on top of PEDOT:PSS coated ITO

DOI: 10.1039/C5RA07161E

by spin-coating $CHCl_3$:toluene solutions (1:1) of **G*n*PYR** and **G*n*TPA** (1.0-2.0% w/v) at a spin speed of 3000 rpm for 30 second to get a 30-40 nm thick of THL/EML. The film thickness was measured by using a Tencor α-Step 500 surface profiler. The BCP/Alq3 layer was deposited on top as electron-transporting layer (ETL)/EML with a thickness of 40-50 nm by evaporation from resistively heated alumina crucible at evaporation rate of 0.5-1.0 nm s^{-1} in vacuum evaporator deposition (ES280, ANS Technology) under a base pressure of ~10^{-5} mbar. The film thickness was monitored and recorded by quartz oscillator thickness meter (TM-350, MAXTEK). A 0.5 nm thick LiF and a 150 nm thick Al layers were the subsequently deposited through a shadow mask on the top of BCP/Alq3 film without braking vacuum to from an active diode areas of 4 mm^2. The measurement of device efficiency was performed according to M. E. Thomson's protocol and the device power efficiencies were calculated using procedure reported previously.[38] Current density-voltage-luminescence (*J-V-L*) characteristics were measured simultaneous by the use of a Keithley 2400 source meter and a Newport 1835C power meter equipped with a Newport 818-UV/CM calibrated silicon photodiode. The EL spectra were recorded by an Ocean Optics USB4000 multichannel spectrometer. All the measurements were performed under ambient atmosphere at room temperature soon after breaking the chamber.

Conclusions

In summary, we have successfully synthesized a series of pyrene- and triphenylamine-functionalized carbazole dendrimers as bifunctional materials for OLEDs. By using carbazole dendrimers (1st and 2nd generations) as a scaffold, we are able to retain the high emissive ability and reduce the excimer emission of pyrene fluorophore in the solid state as well as improve hole-transporting property, amorphous glass-forming ability, solution processability and thermal stability of the material. Particularly, pyrene- and triphenylamine-functionalized 2nd generation carbazole dendrimers, **G2PYR** and **G2TPA**, exhibit a strong blue emission with morphologically and thermally stable amorphous thin films (T_g = 145-211°C). A solution processed blue OLED (ITO/PEDOT:PSS/**G2PYR**(spin coating)/BCP/LiF-Al) using **G2PYR** as an emissive layer shows an excellent luminance efficiency of 5.89 cd A^{-1} (EQE = 6.81%) and a pure blue emission with CIE coordinates of (0.15, 0.16), while Alq3-based green OLED (ITO/PEDOT:PSS/**G2PYR**(spin coating)/Alq3/LiF-Al) using **G2PYR** as hole-transporting layer displays a high luminance efficiency of 6.10 cd A^{-1} (EQE = 1.51%). These results revealed that **G2PYR** is promising as blue emitter and hole-transporter for high efficiency OLEDs with much simpler device architecture. We believe that our results could provide a useful guidance to decorate the highly efficient but planar fluorophore to be suitable for applications in solution-processable and non-doped OLEDs without a hole-transporting layer.

Acknowledgements

This work was supported by the Thailand Research Fund (TRF) (Grant No. DBG5580001 and RTA5680008) and Rayong Institute of Science and Technology (RAIST) Foundation. We thank Department of Physics, Ubon Ratchathani University for providing AFM facility.

Notes and references

[a] Department of Chemistry, Faculty of Science, Ubon Ratchathani University, Ubon Ratchathani 34190, Thailand.

[b] School of Molecular Science and Engineering, Vidyasirimedhi Institute of Science and Technology, Wangchan, Rayong, 21210 Thailand.

[c] National Nanotechnology Center, 130 Thailand Science Park, Klong Luang, Pathumthani 12120, Thailand.

[d] Chemistry Department, Faculty of Science, Chiang Mai University, Chiang Mai 50200, Thailand.

[e] School of Physics, Institute of Science, Suranaree University of Technology, Muang District, Nakhon Ratchasima 30000, Thailand.

† Electronic Supplementary Information (ESI) available: quantum chemical calculation data, CV plot, EL spectra and NMR spectra. See DOI: 10.1039/b000000x/

1 C. H. Chen, J. Shi and C. W. Tang, *Macromol. Symp.*, 1997, **125**, 1; B. W. D'Andrade and S. R. Forrest, *Adv. Mater.*, 2004, **16**, 1585.

2 N. Matsumoto, T. Miyazaki, M. Nishiyama and C. Adachi, *J. Phys. Chem. C*, 2009, **113**, 6261; X. Zhan, Y. Liu, X. Wu, S. Wang and D. Zhu, *Macromolecules*, 2002, **35**, 2529; T. Spehr, R. Pudzich, T. Fuhrmann and J. Salbeck, *Org. Electron.*, 2003, **4**, 61; C. C. Wu, Y. T. Lin, H. H. Chiang, T. Y. Cho, C. W. Chen, K. T. Wong, Y. L. Liao, G. H. Lee and S. M. Peng, *Appl. Phys. Lett.*, 2002, **81**, 577.

3 C. H. Chen and J. M. Shi, *Coord. Chem. Rev.*, 1998, **171**, 161.

4 Y. Hamada, *IEEE. Trans. Electron. Devices*, 1997, **44**, 1208.

5 F. He, H. Xu, B. Yang, Y. Duan, L. Tian, K. Huang, Y. Ma, S. Liu, S. Feng and J. Shen, *Adv. Mater.*, 2005, **17**, 2710; C. Hosokawa, H. Higashi, H. Nakamura and T. Kusumoto, *Appl. Phys. Lett.*, 1995, **67**, 3853.

6 S. L. Lai, Q. X. Tong, M. Y. Chan, T. W. Ng, M. F. Lo, C. C. Ko, S. T. Lee and C. S. Lee, *Org. Electron.*, 2011, **12**, 541; B. Wang, J. Zhao, J. Xiao, C. Cui and R. Liu, *Int. J. Electrochem. Sci.*, 2012, **7**, 2781; T. M. Figueira-Duarte and K. Müllen, *Chem. Rev.*, 2011, **111**, 7260; T. Kumchoo, V. Promarak, T. Sudyoadsuk, M. Sukwattanasinitt and P. Rashatasakhon, *Chem.- Asian J.*, 2010, **5**, 2162; J. Hu and T. Yamato, *Organic Light Emitting Diode-Material, Process and Devices*, InTech, 2011, p 21-60.

7 K. Danel, T. Huang, J. T. Lin, Y. Tao and C. Chuen, *Chem. Mater.*, 2002, **14**, 3860; N. Prachumrak, S. Namuangruk, T. Keawin, S. Jungsuttingwong, T. Sudyoadsuk and V. Promarak, *Eur. J. Org. Chem.*, 2013, **18**, 3825

8 Y. Sato, S. Ichinosawa, T. Ogata, M. Fugono and Y. Murata, *Synth. Met.*, 2000, **111–112**, 25.

9 E. Balasubramaniam, Y. T. Tao, A. Danel and P. Tomasik, *Chem. Mater.*, 2000, **12**, 2788.

10 K.-C. Wu, P.-J. Ku, C.-S. Lin, H.-T. Shih, F.-I. Wu, M.-J. Huang, J.-J. Lin, I.-C. Chen and C.-H. Cheng, *Adv. Funct. Mater.*, 2008, **18**, 67; F. Liu, C. Tang, Q.-Q. Chen, F.-F. Shi, H.-B. Wu, L.-H. Xie, B. Peng, Y. Cao and W. Huang, *J. Phys. Chem. C*, 2009, **113**, 4641.

11 F. Wurthner, C. Thalacker, S. Dieke and C. Tschierske, *Chem.- Eur. J.*, 2001, **7**, 2245; S. A. Jenekhe and J. A. Osaheni, *Science*, 1994, **265**, 765.

12 T. Keawin, C. Sooksai, N. Prachumrak, T. Kaewpuang, D. Muenmart, S. Namuangruk, S. Jungsuttiwong, T. Sudyoadsuk and V. Promarak, *RSC Adv.*, 2015, **5**, 16422.

View Article Online
DOI: 10.1039/C5RA07161E

13 J. K. Salunke, P. Sonar, F. L. Wong, V. A. L. Roy, C. S. Lee and P. P. Wadgaonkar, *Phys. Chem. Chem. Phys.*, 2014, **16**, 23320; P. Sonar, M. S. Soh, Y. H. Cheng, J. T. Henssler and A. Sellinger, *Org. Lett.*, 2010, **12**, 3292; J. Narasimha Moorthy, P. Natarajan, P. Venkatakrishnan, D.-F. Huang and T. J. Chow, *Org. Lett.*, 2007, **9**, 5215.

14 S. Tao, Y. Zhou, C.-S. Lee, X. Zhang and S.-T. Lee, *Chem. Mater.*, 2010, **22**, 2138.

15 K. L. Chan, J. P. F. Lim, X. Yang, A. Dodabalapur, G. E. Jabbour and A. Sellinger, *Chem. Commun*., 2012, **48**, 5106; X. H. Yang, T. Giovenzana, B. Feild, G. E. Jabbour and A. Sellinger, *J. Mater. Chem.*, 2012, **22**, 12689.

16 C. Tang, F. Liu, Y.-J. Xia, J. Lin, L.-H. Xie, G.-Y. Zhong, Q.-L. Fan and W. Huang, *Org. Electron.*, 2006, **7**, 155.

17 A. Thangthong, N. Prachumrak, R. Tarsang, T. Keawin, S. Jungsuttiwong, T. Sudyoadsuk and V. Promarak, *J. Mater. Chem.*, 2012, **22**, 6869.

18 Z. Zhao, X. Xu, H. Wang, P. Lu, G. Yu and Y. Liu, *J. Org. Chem.*, 2008, **73**, 594.

19 M. Y. Lo, C. Zhen, M. Lauters, G. E. Jabbour and A. Sellinger, *J. Am. Chem. Soc.*, 2007, **129**, 5808.

20 X.-H. Zhu, J. Peng, Y. Cao and J. Roncali, *Chem. Soc. Rev.*, 2011, **40**, 3509; L. Duan, L. Hou, T.-W. Lee, J. Qiao, D. Zhang, G. Dong, L. Wang and Y. Qiu, *J. Mater. Chem.*, 2010, **20**, 6392.

21 J. Li, Q. Li and D. Liu, *ACS Appl. Mater. Interfaces*, 2011, **3**, 2099; T. Sudyoadsuk, P. Moonsin, N. Prachumrak, S. Namuangruk, S. Jungsuttiwong, T. Keawin and V. Promarak, *Polym. Chem.*, 2014, **5**, 3982; C. Liu, Q. Fu, Y. Zou, C. Yang, D. Ma and J. Qin, *Chem. Mater.*, 2014, 26, 3074; S.-C. Lo, R. E. Harding, C. P. Shipley, S. G. Stevenson, P. L. Burn and I. D. W. Samuel, *J. Am. Chem. Soc.*, 2009, **131**, 16681; Y. Li, A.-Y.Li, B.-X. Li, J. Huang, L. Zhao, B.-Z. Wang, J.-W. Li, X.-H. Zhu, J. Peng, Y. Cao, D.-G. Ma and J. Roncali, *Org. Lett.*, 2009, **11**, 5318; S.-H. Hwang, C. N. Moorefield and G. R. Newkome, *Chem. Soc. Rev.*, 2008, **37**, 2543.

22 W. L. Jia, D. R.;Bai, T. McCormick, Q. D. Liu, M. Motala, R. Y. Wang, C. Seward, Y. Tao and S. Wang, *Chem. Eur. J.*, 2004, **4**, 994; P. C. Bevilacqua, R. Kierzek, K. A. Johnson and D. H. Turner, *Science*, 1992, **258**, 1355.

23 P. Moonsin, N. Prachumrak, R. Rattanawan, T. Keawin, S. Jungsuttiwong, T. Sudyoadsuk and V. Promarak, *Chem. Commun.*, 2012, **48**, 3382.

24 P. Thongkasee, A. Thangthong, N. Janthasing, T. Sudyoadsuk, S. Namuangruk, T. Keawin, S. Jungsuttiwong and V. Promarak, *ACS Appl. Mater. Interfaces*, 2014, **6**, 8212.

25 R. Schmechel and H. von Seggern, *Phys. Stat. Sol. (A)*, 2004, **201**, 1215.

26 M. J. Frisch, G. W. Trucks, H. B. Schlegel, G. E. Scuseria, M. A. Robb, J. R. Cheeseman, G. Scalmani, V. Barone, B. Mennucci, G. A. Petersson, H. Nakatsuji, M. Caricato, X. Li, H. P. Hratchian, A. F. Izmaylov, J. Bloino, G. Zheng, J. L. Sonnenberg, M. Hada, M. Ehara, K. Toyota, R. Fukuda, J. Hasegawa, M. Ishida, T. Nakajima, Y. Honda, O. Kitao, H. Nakai, T. Vreven, J. A. Montgomery, Jr, J. E. Peralta, F. Ogliaro, M. Bearpark, J. J. Heyd, E. Brothers, K. N. Kudin, V. N. Staroverov, R. Kobayashi, J. Normand, K. Raghavachari, A. Rendell, J. C. Burant, S. S. Iyengar, J. Tomasi, M. Cossi, N. Rega, J. M. Millam, M. Klene, J. E. Knox, J. B. Cross, V. Bakken, C. Adamo, J. Jaramillo, R. Gomperts, R. E. Stratmann, O. Yazyev, A. J. Austin, R. Cammi, C. Pomelli, J. W. Ochterski, R. L. Martin, K. Morokuma, V. G. Zakrzewski, G. A. Voth, P. Salvador, J. J. Dannenberg, S. Dapprich, A. D. Daniels, ¨O. Farkas, J. B. Foresman, J. V. Ortiz, J. Cioslowski, and D. J. Fox, *Gaussian 09*, Revision A.1, Gaussian Inc., Wallingford CT, 2009.

27 Z. J. Ning, Y. C. Zhou, Q. Zhang, D. G. Ma, J. J. Zhang and H. Tian, *J. Photochem. Photobiol. A*, 2007, **192**, 8.

28 P. Strohriegl and J. V. Grazulevicius, *Adv. Mater.*, 2002, **14**, 1439; R. Fink, Y. Heischkel, M. Thelakkat, H.-W. Schmidt, C. Jonda and M. Hüppauff, *Chem. Mater.*, 1998, **10**, 3620.

29 W. Kim, G. Kushto, G. Kim and Z. Kafafi, *J. Polym. Sci. B: Polym. Phys.*, 2003, **41**, 2522; S. T. Zhang, Z. J. Wang, J. M. Zhao, Y. Q. Zhan, Y. Wu, Y. C. Zhou, X. M. Ding and X. Y. Houa, *Appl. Phys. Lett.*, 2004, **84**, 2916.

30 D. Y. Kim, H. N. Cho and C. Y. Kim, *Prog. Polym. Sci.*, 2000, **25**, 1089.

31 U. Mitschke and P. Bäuerle, *J. Mater. Chem.*, 2000, **10**, 1471.

32 Y. K. Kim and S.-H. Hwang, *Synth. Met.*, 2006, **156**, 1028; C.-H. Chen, W.-J. Shen, K. Jakka and C.-F. Shu, *Synth. Met.*, 2004, **143**, 215; A. M. Thaengthong, S. Saengsuwan, S. Jungsuttiwong, T. Keawin, T. Sudyoadsuk and V. Promarak, *Tetrahedron Lett.*, 2011, **37**, 4749.

33 J. Zhuang, W. Li, W. Su, Y. Liu, Q. Shen, L. Liao and M. Zhou, *Org. Electron.*, 2013, **14**, 2596; F. Kessler, Y. Watanabe, H. Sasabe, H. Katagiri, M. K. Nazeeruddin, M. Grätzel and J. Kido, *J. Mater. Chem. C*, 2013, **1**, 1070.

34 S. Wu, M. Aonuma, Q. Zhang, S. Huang, T. Nakagawa, K. Kuwabara and C. Adachi, *J. Mater. Chem. C*, 2014, **2**, 421.

35 W.-L. Jia, T. M. Cormick, Q.-D. Liu, H. Fukutani, M. Motala, R.-Y. Wang, Y. Tao and S. Wang, *J. Mater. Chem.*, 2004, **14**, 334.

36\. A. M. Thangthong, D. Meunmart, N. Prachumrak, S. Jungsuttiwong, T. Keawin, T. Sudyoadsuk and V. Promarak, *Chem. Commun.*, 2011, **47**, 7122; P. Moonsin, N. Prachumrak, S. Namuangruk, S. Jungsuttiwong, T. Keawin, T. Sudyoadsuk and V. Promarak, *J. Mater. Chem. C*, 2014, **2**, 5540.

37 T. Sudyoadsuk, S. Pansay, S. Morada, R. Rattanawan, S. Namuangruk, T. Kaewin, S. Jungsuttiwong and V. Promarak, *Eur. J. Org. Chem.*, 2013, **23**, 5051.

38 S. R. Forrest, D. D. C. Bradley and M. E. Thomson, *Adv. Mater.*, 2003, **15**, 1043.

View Article Online
DOI: 10.1039/C5RA07161E

Graphical Abstract

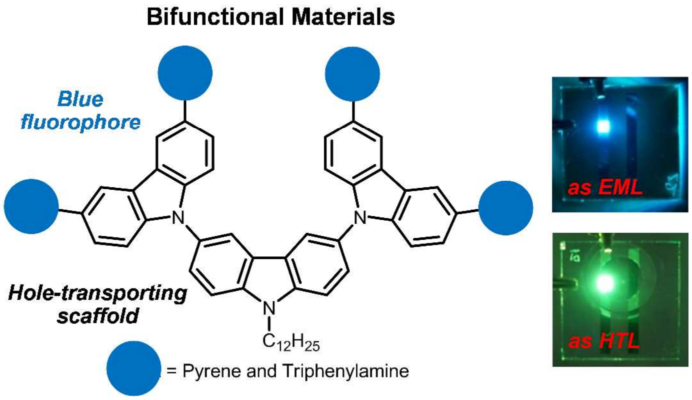

Solution processed blue OLED using these molecules as an emissive layer show an excellent luminance efficiency of 5.89 cd A^{-1} (EQE = 6.81%) and a pure blue emission with CIE coordinates of (0.15, 0.16), while Alq3-based green OLEDs using these molecules as a hole-transporting layer display a high luminance efficiency of 6.10 cd A^{-1} (EQE = 1.51%), indicating they are promising bifunctional materials for high efficiency OLEDs with much simpler device architecture.